RESEARCH MEMORANDUM

FREE-FLIGHT INVESTIGATION AT TRANSONIC SPEEDS OF THE

STABILITY CHARACTERISTICS OF A TAILLESS MISSILE

CONFIGURATION HAVING A 45° SWEPTBACK WING

OF ASPECT RATIO 4

By Richard G. Arbic

Langley Aeronautical Laboratory
Langley Field, Va.

NATIONAL ADVISORY COMMITTEE
FOR AERONAUTICS
WASHINGTON

August 28, 1956

NATIONAL ADVISORY COMMITTEE FOR AERONAUTICS

RESEARCH MEMORANDUM

FREE-FLIGHT INVESTIGATION AT TRANSONIC SPEEDS OF THE

STABILITY CHARACTERISTICS OF A TAILLESS MISSILE

CONFIGURATION HAVING A 45° SWEPTBACK WING

OF ASPECT RATIO 4

By Richard G. Arbic

SUMMARY

A flight test of a long-range missile configuration having a 45° sweptback wing of aspect ratio 4 was conducted between Mach numbers of 0.85 and 1.3 and a Reynolds number range of 3.6×10^6 to 7.4×10^6. Lateral pulse inputs resulted in combined longitudinal and lateral motions which were analyzed separately by a two-degree-of-freedom method for the longitudinal case and a three-degree-of-freedom vector method for the lateral case to obtain static and dynamic stability derivatives.

The longitudinal flexible-wing results indicated a gradual transonic trim change and a lift-curve slope comparable with that for the same configuration with a wing of aspect ratio 5.5. Lateral derivatives were in reasonable agreement with referenced data for the higher Mach numbers but were thought to be slightly low for the lower test Mach numbers.

INTRODUCTION

The Langley Pilotless Aircraft Research Division has investigated the transonic low-lift aerodynamic characteristics of a long-range swept-wing missile configuration designed to cruise at high subsonic Mach numbers and to attain supersonic speeds during the terminal approach to the target. The missile has a wing, body, and vertical tail but has no horizontal tail. The wing has 45° sweepback, an aspect ratio of 5.5, and a taper ratio of 0.4. The airfoil section is 6 percent thick streamwise and is slightly drooped at the leading edge.

Two rocket-propelled models have been tested to determine the longitudinal stability characteristics of this missile configuration and the

results of these tests are presented in reference 1. This paper presents
the results of an additional rocket-propelled-model test which was made to
determine the lateral stability characteristics of the configuration. The
model used for this test was modified, however, to reduce the wing aspect
ratio to 4.0. This reduction in aspect ratio was accomplished simply by
removing a portion of the tip section from a standard aspect-ratio-5.5
wing. The purpose of the modification was to provide comparative infor-
mation on a configuration which could be expected to have better aeroelas-
tic characteristics than those of the aspect-ratio-5.5 configuration.

The pulse-rocket technique was used throughout the flight of the
present model to obtain longitudinal as well as lateral oscillations
from which stability derivatives could be determined. The results
obtained from this test are presented in comparison with the longitudinal
derivatives obtained in reference 1 for the aspect-ratio-5.5 configura-
tion and also in comparison with longitudinal and lateral derivatives
obtained from wind-tunnel tests of the configuration having wings of
both aspect ratio 4 and 5.5 (ref. 2).

SYMBOLS

Dimensions used for the coefficients and derivatives are the total
wing area (2.84 sq ft), the mean aerodynamic chord (0.867 ft), and the
wing span (3.382 ft). A sketch of the axes system used is shown in
figure 1.

a lateral damping factor (logarithmic decrement of Dutch-roll
oscillation defined as being a positive number for a damped
oscillation)

b wing span, ft; also longitudinal damping factor, positive for
damped oscillation

c local wing chord, ft.

$\bar{c}$ wing mean aerodynamic chord, ft.

c_r root chord of wing at model center line, ft.

c.g.   center of gravity of model

I_X moment of inertia in roll with respect to principal axes,
slug-ft^2

I_Z moment of inertia in yaw with respect to principal axes,
slug-ft^2

I_Y moment of inertia in pitch with respect to principal axes, slug-ft^2

I_{XZ} product of inertia (zero for present test), slug-ft^2

L applied load, lb

M Mach number or pitching moment

m mass of model, $\dfrac{W}{32.2}$, slugs

N normal force, lb

P period, sec

p angular rolling velocity, radians/sec

q dynamic pressure, lb/ft^2 or pitching velocity, radians/sec

r yawing angular velocity, radians/sec

S total wing area, sq ft

V velocity, ft/sec

W model weight, lb

y spanwise distance from model center line, ft

$\dfrac{y}{b/2}$ nondimensional spanwise parameter

α angle of attack, measured from projection of relative wind to fuselage reference axis, deg or radians

β angle of sideslip, measured from relative wind to fuselage reference axis, deg or radians

θ angle of pitch, deg; also local wing twist angle, deg

ϕ angle of roll, deg or radians

ψ angle of yaw, radians

ω frequency of Dutch roll oscillation, radians/sec

ω_0 undamped natural circular frequency, $\left(\omega^2 + a^2\right)1/2$

C_N normal-force coefficient, $\dfrac{\text{Normal force}}{qS}$

C_{N_α} normal-force-curve slope per degree, $\dfrac{\partial C_N}{\partial \alpha}$

C_m pitching-moment coefficient, $\dfrac{\text{Pitching moment}}{qS\bar{c}}$

C_{m_α} static stability parameter per degree

$C_{m_q} + C_{m_{\dot{\alpha}}}$ sum of pitch damping coefficients per radian, $\dfrac{\partial C_m}{\partial \dfrac{\dot{\theta}\bar{c}}{2V}} + \dfrac{\partial C_m}{\partial \dfrac{\dot{\alpha}\bar{c}}{2V}}$

C_l rolling-moment coefficient, $\dfrac{\text{Rolling moment}}{qSb}$

C_{l_β} effective dihedral derivative per radian, $\dfrac{\partial C_l}{\partial \beta}$

C_{l_p} damping-in-roll derivative per radian, $\dfrac{\partial C_l}{\partial \dfrac{pb}{2V}}$

C_{l_r} rate of change of rolling-moment coefficient with yawing angular-velocity factor per radian, $\dfrac{\partial C_l}{\partial \dfrac{rb}{2V}}$

C_n yawing-moment coefficient, $\dfrac{\text{Yawing moment}}{qSb}$

C_{n_β} directional stability derivative per radian, $\dfrac{\partial C_n}{\partial \beta}$

C_{n_r} rate of change of yawing-moment coefficient with yawing angular-velocity factor per radian, $\dfrac{\partial C_n}{\partial \dfrac{rb}{2V}}$

$C_{n_{\dot{\beta}}}$ rate of change of yawing-moment coefficient with rate of change of angle-of-sideslip factor per radian, $\dfrac{\partial C_n}{\partial \dfrac{\dot{\beta}b}{2V}}$

C_{n_p} rate of change of yawing-moment coefficient with rolling-velocity factor per radian, $\dfrac{\partial C_n}{\partial \dfrac{pb}{2V}}$

C_Y lateral-force coefficient, $\dfrac{\text{Lateral force}}{qS}$

C_{Y_β} lateral-force-curve slope per radian, $\dfrac{\partial C_Y}{\partial \beta}$

A dot over a variable indicates the first derivative of the variable with respect to time. Two dots indicate the second derivative. The symbol $|\ |$ denotes the absolute magnitude of the quantity within the symbol. Phase angles are indicated by subscript notation as $\Phi_{\ddot{\phi}\beta}$ which means the phase angle between the rolling acceleration and the angle of sideslip where the second subscript symbol is used as the reference.

MODEL AND INSTRUMENTATION

A three-view sketch of the model is presented as figure 2. The portion of the wing tips cut off of the aspect-ratio-5.5 wing to form the aspect-ratio-4 wing of the present test is shown by dashed lines. The wing was swept back 45° at the 40.6-percent streamwise chord line and had a taper ratio of 0.52. A photograph of the model is presented as figure 3. Table I presents the physical characteristics of the model, and table II gives the wing, body, and vertical-tail ordinates. The model fuselage had a fineness ratio of 13.94 and was of sheet-aluminum construction. The wing and vertical tail were machined from solid 75S-T6 aluminum alloy and solid magnesium, respectively.

The model contained six pulse rockets located on the fuselage center-line in such a manner as to produce yaw, sideslip, and roll-input disturbances. The roll disturbance was caused by the fact that the model vertical center of gravity was slightly above the model center line. The longitudinal center of gravity of the model was at 6 percent of the mean aerodynamic chord forward of the leading edge of the mean aerodynamic chord.

Model instrumentation consisted of a six-channel telemeter which transmitted continuous values of normal, transverse, and rolling acceleration, angle of attack, angle of sideslip, and static pressure. Model velocity was obtained by use of a CW Doppler radar unit and trajectory data were obtained by an NACA modified SCR 584 radar tracking unit. Atmospheric conditions were obtained from a radiosonde balloon released shortly after the flight test. An indication of the roll rate of the model was obtained by means of rollsonde equipment which measures the angular velocity of the polarized telemeter signal. Motion-picture cameras were used to photograph the model during flight.

TESTS AND CORRECTIONS

The model was accelerated to maximum velocity by an ABL deacon rocket motor and data were obtained during coasting flight of the model following separation from the booster. The model was disturbed by periodic firing of the pulse rockets. Reynolds number and dynamic-pressure data for the test are shown as a function of Mach number in figure 4. The Reynolds number range for this test is 3.6×10^6 to 7.4×10^6 and the dynamic-pressure range is approximately 700 to 2,400 pounds per square foot. Whenever possible, the results from this test are compared with results from the rocket-model test of reference 1 and the wind-tunnel test of reference 2; therefore, for purposes of comparison, the Reynolds number and dynamic-pressure ranges for these references are also shown in figure 4. The present model was flight tested at the Langley Pilotless Aircraft Research Station at Wallops Island, Va.

Angle-of-attack and angle-of-sideslip data were corrected to the model center of gravity by the method shown in reference 3. The CW Doppler radar velocity data were corrected for the effect of winds at altitude and for curvature of the model flight path. The relatively low natural frequency of the roll angular accelerometer necessitated a correction of the phase angle between $\ddot{\phi}$ and β which amounted to approximately 8° at a Mach number of 0.8 and 17° at a Mach number of 1.3. This correction corresponded to a constant time lag of 0.01 second.

Prior to the flight test, the wing and vertical tail of the model were static tested by application of loads at various spanwise stations to obtain structural influence coefficients. The influence coefficients thus obtained are presented in figures 5 and 6 to give an indication of the flexibility of the wing and vertical tail. Flexibility corrections were not applied to the results presented herein, but the data of figures 4, 5, and 6 will permit such corrections to be made.

ANALYSIS

Time histories of Mach number, angle of attack, angle of sideslip, and rolling acceleration are presented in figure 7. Roll data available are not of sufficient accuracy to permit a five-degree-of-freedom analysis. Information presented in reference 4 and 5 indicates that the longitudinal and lateral motions may be treated independently when low values of inertial coupling terms exist. For these reasons, suitable portions of the oscillations were analyzed separately. The two-degree-of-freedom method of reference 6 was used to obtain longitudinal derivatives and the time-vector method of references 4 and 5 was used to determine lateral derivatives.

Typical vector plots of the lateral equations of motion are presented in figure 8. In order to close the vector diagram for the rolling-moment equation, it was necessary to estimate values of either C_{l_r} or C_{l_p}. Because of the relative difficulty of estimating the derivative C_{l_r}, values of C_{l_p} were used as obtained from an unpublished rocket-propelled model test of a transonic wing design of similar plan form. The derivatives then obtainable from the rolling-moment-equation were C_{l_r} and C_{l_β}. The vector solution of the yawing-moment equation was obtained for assumed values of C_{n_p} of 0, 0.1, and -0.1. The derivatives obtainable from this equation were C_{n_β} and $C_{n_r} - C_{n_{\dot{\beta}}}$. From the vector diagram for the yawing-moment equation, it can be seen that the value of C_{n_p} has little effect on C_{n_β} but has a large effect on the derivatives $C_{n_r} - C_{n_{\dot{\beta}}}$.

For the present test configuration, measurements by the oscillating-pendulum method indicated that the inclination of the principal axis was coincident with the body axis. As a result, the product-of-inertia terms in the lateral equations of motion were zero.

ACCURACY

The maximum probable errors for some of the test results are listed in the following table and are based on accepted ranges of accuracy for the various instruments and experience from tests of similar models.

	M = 0.8	M = 1.3
Mach number	±0.010	±0.007
Angle of attack, deg	±0.4	±0.4
Angle of sideslip, deg	±0.4	±0.4
Normal-force coefficient	±0.009	±0.003
Side-force coefficient	±0.009	±0.003
Rolling acceleration, deg/sec^2	±7.5	±7.5

Reference 4 presents an analysis of the accuracy of results obtainable by vector method for one specific configuration. It is believed that the percentages quoted for the various quantities and coefficients are fairly representative of the degree of accuracy for the same quantities and coefficients for the present test configuration. Any deviations or inaccuracies in the coefficients resulting from the assumption of independent longitudinal and lateral motions are over and above the percentages quoted in reference 4.

RESULTS AND DISCUSSION

The basic motions in angle of attack, angle of sideslip, and rolling acceleration are presented in figure 7, and results of the analysis of these motions are presented in figures 9 to 19. For convenience, the periods of time during which pulse rockets were firing are indicated on figure 7. Note should be made of the fact that the initial response of the model to the third, fourth, and fifth pulse rockets was different than the initial response to the other pulse rockets. These particular pulse rockets were located nearest the wing trailing edge as shown in figure 2. All the pulse rockets were mounted so as to produce initially a positive sideslip disturbance and a negative roll disturbance. Pulses 4 and 5, however, produced negative sideslip disturbances and each of the three forward pulse rockets (rockets 3, 4, and 5) produced positive roll disturbances. The angle-of-attack response to these three pulses was also negative, whereas it was positive for pulses 1 and 6. It is believed that the above excursions are a result of the influence of the pulse-rocket jet acting beneath the left-wing panel.

Trim Characteristics

Figure 9 presents the longitudinal and lateral trim characteristics of the model. The trim angle of attack and angle of sideslip were obtained as the mean line of the envelopes of angle of attack and angle of sideslip shown in figure 7, and the trim normal-force and side-force

coefficients were obtained in a like manner from plots of the normal-force and side-force coefficients.

The trim angle of attack and trim normal-force coefficient are near zero and vary only slightly throughout the Mach number range of the test. The general level of trim values exhibited by the lateral data (0.5° in β and -0.002 in C_Y) are believed to be the result of constructional asymmetries since both the rollsonde data and photographic evidence indicate negligible steady-state roll. The abrupt trim change indicated between Mach numbers of 0.9 and 1.0 is believed to be the result of test conditions previously discussed (see fig. 7) and is not necessarily a true trim change.

Lift and Longitudinal Stability

Lift.- Basic plots of normal-force coefficient against angle of attack are shown in figure 10. The curves are linear over the range of normal-force coefficients shown and are free of hysteresis. This condition indicates that the normal-force data were essentially unaffected by lateral motions occurring at the time.

The normal-force-curve slope is shown in figure 11 and is compared with lift-curve slopes from the rocket-propelled-model test of reference 1 and from the wind-tunnel test of reference 2. The derivatives are based on the respective areas of the individual wings, and the normal-force and lift-curve slopes are comparable because of the small angles of attack involved. Both the aspect-ratio-4 and aspect-ratio-5.5 rocket model data are lower than the comparable wind-tunnel data. The major portion of this difference can be attributed to wing flexibility.

It is interesting to note the inverse effect of reduced aspect ratio indicated by the rocket-model tests at supersonic speeds as compared with the usual result of reduced lift-curve slope with reduced aspect ratio as shown by the wind-tunnel tests. This effect results from reducing the aspect ratio by cutting off the wing-tip sections which are the most flexible portions of the wing panels.

Static stability.- The static stability parameter C_{m_α} was computed from the faired curve of the periods of the longitudinal oscillations shown in figure 12(a). The scatter in the period data could indicate some influence of the lateral motion upon the longitudinal motion; however, the faired curve is a good indication of the magnitude and variation of the longitudinal period with Mach number. Figure 12(b) shows the variation of the C_{m_α} data with Mach number for the center of gravity located at 6 percent of the mean aerodynamic chord forward of the leading edge of the mean aerodynamic chord.

The aerodynamic-center location is shown in figure 13 and is compared with results from reference 2 for the aspect-ratio-4 wing. Again, the effect of wing flexibility is shown by the more forward location of the aerodynamic center for the present test model particularly at supersonic speeds.

The aerodynamic-center location of the aspect-ratio-4 configuration is compared with that for the aspect-ratio-5.5 configuration in figure 14. Aerodynamic-center locations are plotted in percent of the root chord back of the leading edge of the root chord in order to provide a common reference for the aerodynamic center of the two wing configurations. The forward movement of the aerodynamic center is less severe at supersonic speeds for the aspect-ratio-4 wing than for the aspect-ratio-5.5 wing.

Dynamic stability.- Figure 15 presents the longitudinal total damping factor b and the sum of the pitch damping coefficients $C_{m_q} + C_{m_{\dot\alpha}}$. The total damping is greatest for the higher Mach numbers. The sum of the pitch damping coefficients is slightly unstable (positive) near Mach number 0.96 and above Mach number 1.25, but the total damping remains stable throughout the test range. Although values for the derivative $C_{m_q} + C_{m_{\dot\alpha}}$ may be applied directly to the full-scale missile, the total damping obtained in this rocket-propelled model test is not necessarily indicative of the total damping of the full-scale missile.

Side-Force and Lateral Stability

Basic lateral data.- Basic plots of side-force coefficient against angle of sideslip are shown in figure 16. There is more scatter and hysteresis apparent in these curves than in the basic curves of normal-force coefficient in figure 10. Examination of figure 17(a) also reveals that considerably more scatter exists in the lateral-period data than in the longitudinal-period data particularly for the lower Mach numbers. These conditions probably indicate that the lateral motions were more influenced by longitudinal motions existing at the time than were the longitudinal motions by the existing lateral motions.

The lateral damping factor a is shown in figure 17(b), and phase and amplitude relationships between rolling acceleration and angle of sideslip are shown in figure 18 together with the undamped natural circular frequency. These characteristics of the Dutch roll oscillation are presented to show the magnitude and variation with Mach number, but it should be pointed out that these relationships represent the dynamic characteristics of only the subject rocket model and do not necessarily indicate the characteristics of a full-scale missile.

Sideslip derivatives.- The sideslip derivatives are presented in figure 19 and are compared with the corresponding derivatives from reference 2 and unpublished wind-tunnel data. Both the data of reference 2 and the unpublished data are for the aspect-ratio-5.5 configuration. Similar data are not available for the aspect-ratio-4 configuration.

The values of C_{Y_β} in figure 19 were obtained as the slope of the basic curves of C_Y against β of which the curves in figure 16 are typical. The derivative C_{n_β} is shown as obtained from both the vector method and a single-degree-of-freedom calculation using the faired curve of the periods of the lateral oscillations. The curve obtained from the vector method is for $C_{n_p} = 0$. The values of C_{n_β} for values of $C_{n_p} = 0.1$ and -0.1 are not shown since C_{n_p} has little effect on the value of C_{n_β}. This can be seen by examination of the typical vector plot for the yawing-moment equation in figure 8. Results of the vector solution for the derivative C_{l_β} are compared with wind-tunnel results in figure 19(c). As previously mentioned in the Analysis, the present test values of C_{l_β} are dependent on the estimated values of C_{l_p} shown in figure 20(c). These estimates were based on unpublished experimental rocket-propelled model data for a transonic wing design which had an aspect ratio of 4, a taper ratio of 0.6, and leading-edge sweep of 46.7°.

Some discussion is in order regarding the comparisons between the present-test values of the sideslip derivatives and the wind-tunnel values. First, it should be noted that the referenced and unpublished data are based on the dimensions of the aspect-ratio-5.5 wing. Conversion of these data to the dimensions of the aspect-ratio-4 wing would increase the values for C_{Y_β} by a factor of 1.15 and the values of C_{n_β} and C_{l_β} by a factor of 1.44. Secondly, the present test values of the derivatives are for a model having a flexible vertical tail and are therefore low in magnitude, especially for the higher Mach numbers and dynamic pressures. Consequently, it is thought that the data are in fairly good agreement at the higher Mach numbers but that the present test values of the sideslip derivatives may be somewhat low for the lower Mach numbers when compared with the wind-tunnel results. This may be an indication of longitudinal influence upon the lateral mode of motion to such a degree as to introduce some inaccuracies for the lower Mach numbers. Examination of the time history (fig. 7) would tend to bear this out, for it is seen that the magnitude of the angle of attack has increased for the pulse rocket disturbances between Mach numbers 0.85 and 0.95 and the angle of sideslip and rolling acceleration are fairly erratic in this region.

Moment derivatives due to yawing.- Figure 20 presents the rolling-moment-due-to-yawing derivatives C_{l_r}, the damping-in-yaw derivative $C_{n_r} - C_{n_{\dot{\beta}}}$, and the estimated damping-in-roll derivative C_{l_p}. The variation with Mach number for C_{l_r} is similar to that for the static derivatives C_{Y_β} and C_{n_β}, a maximum value being near Mach number 1.1. The derivative $C_{n_r} - C_{n_{\dot{\beta}}}$ is shown for the three assumed values of C_{n_p}, and the value of C_{n_p} is seen to have a marked effect on the value of $C_{n_r} - C_{n_{\dot{\beta}}}$. However, the damping in yaw is stable for the entire range of C_{n_p} values between 0.1 and -0.1.

SUMMARY OF RESULTS

A flight test of an aspect-ratio-4 swept-wing missile configuration between Mach numbers of 0.85 and 1.3 resulted in both longitudinal and lateral motions. These motions were analyzed separately by a two-degree-of-freedom method for the longitudinal case, and a three-degree-of-freedom vector method for the lateral case. The flight tests and comparisons with referenced rocket-propelled model and wind-tunnel data indicated the following results:

1. Values of trim angle of attack and normal-force coefficient were near zero and indicated a gradual transonic trim change. A fairly abrupt lateral trim change was indicated near Mach number 1.0, but it was thought that this test did not prove conclusively that the condition would exist under different test conditions.

2. At high dynamic pressures, values of the lift-curve slope were slightly higher than those for the same configuration having a wing of the same material and an aspect ratio of 5.5.

3. Forward movement of the aerodynamic center was less severe at supersonic speeds for the aspect-ratio-4 configuration than for the aspect-ratio-5.5 configuration.

4. Lateral derivatives for which comparative reference data are available were in reasonable agreement for the higher test Mach numbers but were thought to be slightly low for the lower Mach numbers.

Langley Aeronautical Laboratory,
    National Advisory Committee for Aeronautics,
        Langley Field, Va., April 30, 1956.

REFERENCES

1. Arbic, Richard G., and Gillespie, Warren, Jr.: Free-Flight
   Longitudinal-Stability Investigation Including Some Effects of
   Wing Elasticity From Mach Numbers of 0.85 to 1.34 of a Tailless
   Missile Configuration Having a 45° Sweptback Wing of Aspect Ratio 5.5.
   NACA RM L53F18, 1953.

2. Phelps, E. Ray, and Lazzeroni, Frank A.: Wind-Tunnel Investigation
   of the Aerodynamic Characteristics of a 1/15-Scale Model of the
   Northrop MX-775A Missile. NACA RM A51E28, 1951.

3. Ikard, Wallace L.: An Air-Flow-Direction Pickup Suitable for Teleme-
   tering Use on Pilotless Aircraft. NACA RM L53K16, 1954.

4. Mitchell, Jesse L, and Peck, Robert F.: Investigation of the Lateral
   Stability Characteristics of the Douglas X-3 Configuration at Mach
   Numbers From 0.6 to 1.1 by Means of a Rocket-Propelled Model.
   NACA RM L54L20, 1955.

5. D'Aiutolo, Charles T., and Henning, Allen B.: Lateral Stability
   Characteristics at Low Lift Between Mach Numbers of 0.85 and 1.15
   of a Rocket-Propelled Model of a Supersonic Airplane Configuration
   Having a Tapered Wing With Circular-Arc Sections and 40° Sweepback.
   NACA RM L55A31, 1955.

6. Gillis, Clarence L., Peck, Robert F., and Vitale, A. James.: Pre-
   liminary Results From a Free-Flight Investigation at Transonic and
   Supersonic Speeds of the Longitudinal Stability and Control Charac-
   teristics of an Airplane Configuration With a Thin Straight Wing of
   Aspect Ratio 3. NACA RM L9K25a, 1950.

TABLE I

PHYSICAL CHARACTERISTICS OF THE MODEL

Wing:
    Area, sq ft 2.84
    Span, ft 3.382
    Aspect ratio 4.02
    Mean aerodynamic chord, ft 0.867
    Sweepback of 0.406-chord line, deg   45
    Dihedral, deg   0
    Taper ratio, Tip chord/Root chord 0.52

Vertical tail:
    Area (extended to center line), sq ft 0.45
    Span (from fuselage center line), ft   1
    Sweepback of 0.4-chord line, deg   33
    Taper ratio 0.286

Fuselage:
    Length, ft 6.74
    Maximum diameter, ft 0.483
    Fuselage fineness ratio, Length/Diameter 13.94
    Nose fineness ratio 4.14
    Boattail fineness ratio 2.76

Weight and balance:
    Weight, lb 73.0
    Wing loading, lb/sq ft 25.8
    Center-of-gravity position, percent $\bar{c}$ forward of
      leading edge of $\bar{c}$ 6
    Moment of inertia in pitch, I_Y, slug-ft^2 . . . .   6.88
    Moment of inertia in yaw, I_Z, slug-ft^2 . . . .   7.22
    Moment of inertia in roll, I_X, slug-ft^2 . . . .   0.405
    Product of inertia, I_{XZ}, slug-ft^2   0
    Inclination of principal axis, deg   0

TABLE II

BODY, WING, AND VERTICAL-TAIL ORDINATES

Body Ordinates

Station, in. from nose	Radius, in.
0	0
1.4	.380
2.0	.548
4.0	1.066
6.0	1.502
8.0	1.857
10.0	2.151
12.0	2.390
14.0	2.575
17.0	2.770
20.0	2.878
22.0	2.900
Straight line	
65.0	2.900
68.0	2.875
70.0	2.810
72.0	2.700
74.0	2.545
76.0	2.340
78.0	2.070
80.0	1.710
80.9	1.500

Wing Ordinates

Station, percent chord	Upper wing, percent chord	Lower wing, percent chord
0	-0.850	0.850
1.25	.200	1.573
2.50	.610	1.855
5.00	1.120	2.190
7.50	1.480	2.410
10.00	1.773	2.567
15.00	2.227	2.782
20.00	2.532	2.922
25.00	2.747	2.998
30.00	2.900	3.033
35.00	2.980	3.040
40.00	3.010	3.020
50.00	2.855	2.860
60.00	2.380	2.380
70.00	1.812	1.812
80.00	1.233	1.233
90.00	.640	.640
100.00	.015	.015

Vertical-Tail Ordinates

Station, percent chord	Upper and lower tail, percent chord
0	0
1.25	.960
2.50	1.335
5.00	1.770
7.50	2.060
10.00	2.265
15.00	2.567
20.00	2.770
25.00	2.907
30.00	3.010
40.00	3.120
50.00	3.057
60.00	2.810
70.00	2.395
75.00	2.090
Straight line	
100.00	.100

Body-axes system used for lateral analysis.
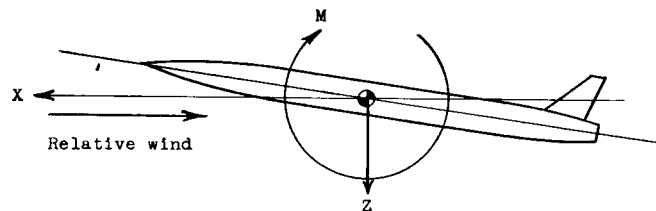
Stability-axes system used for longitudinal analysis.

Figure 1.- Sketch showing stability- and body-axes system used for analysis. Arrows indicate positive direction of forces, moments, and angles.
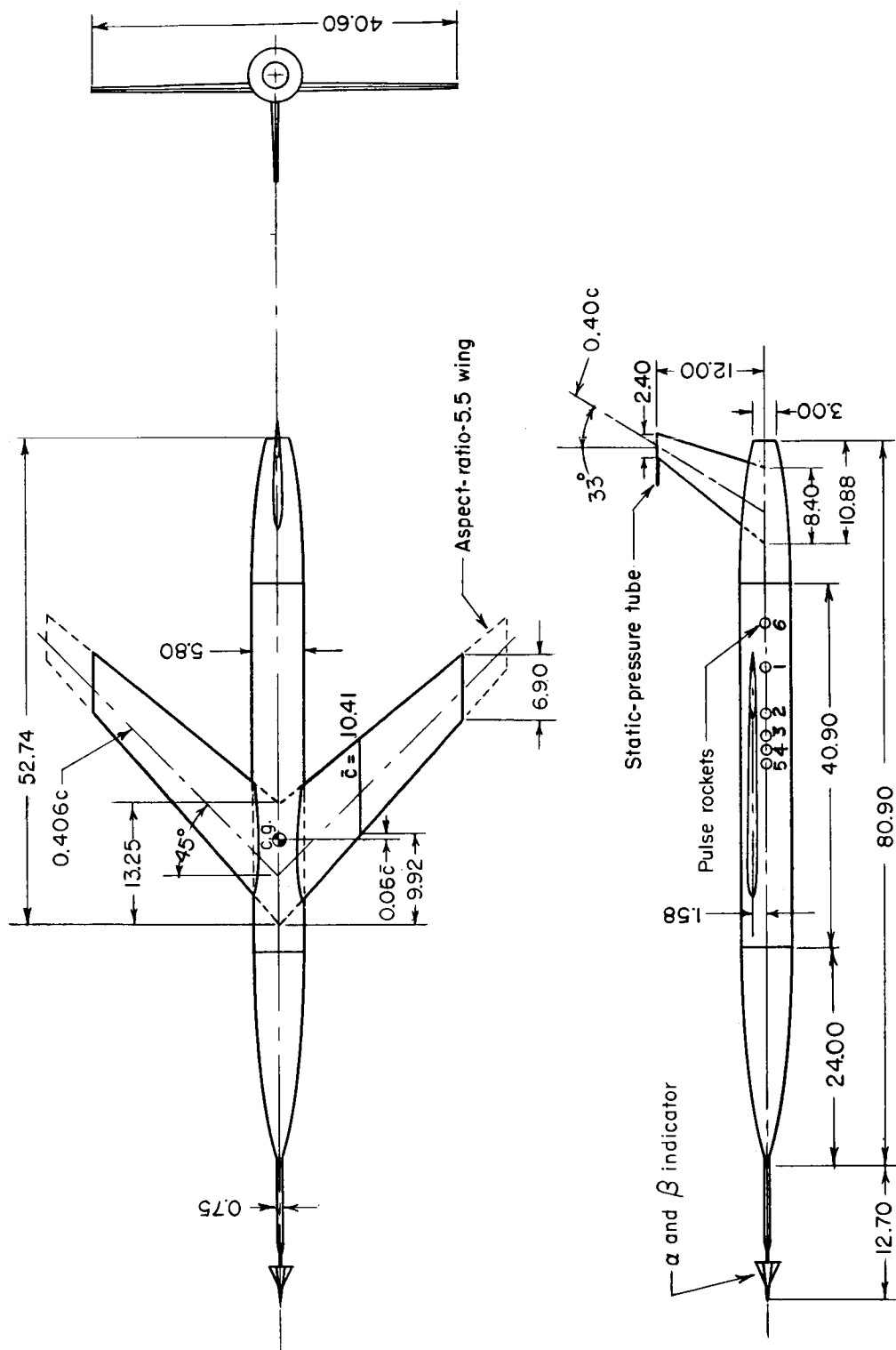
Figure 2.- General arrangement of the test model. All dimensions are in inches.
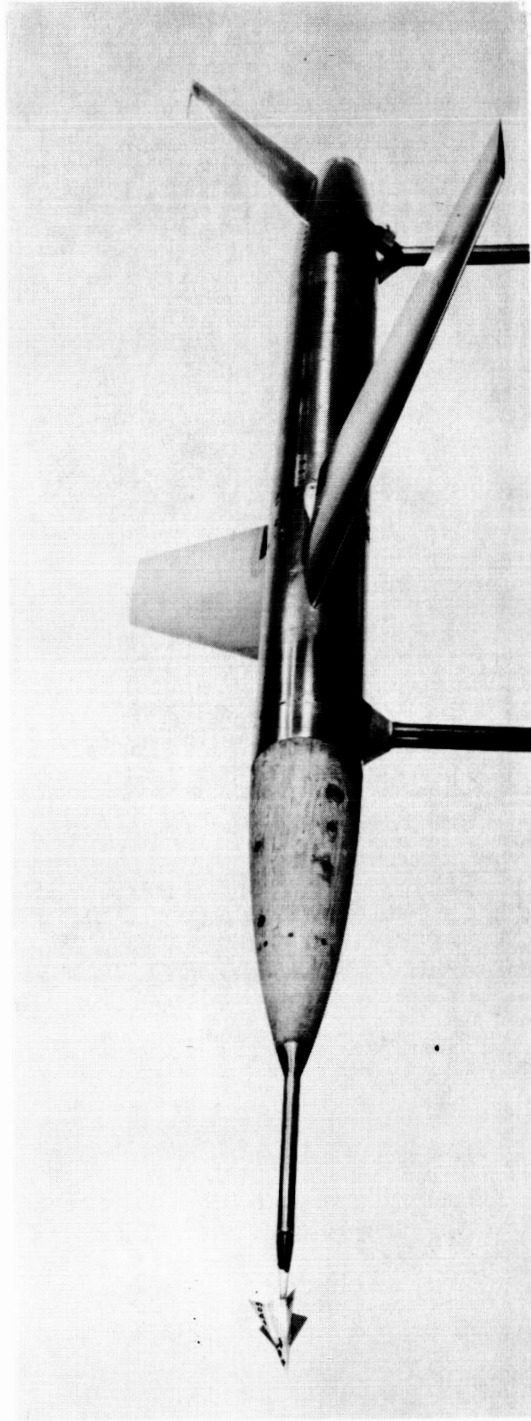
L-85120

Figure 3.- Photograph of the model.
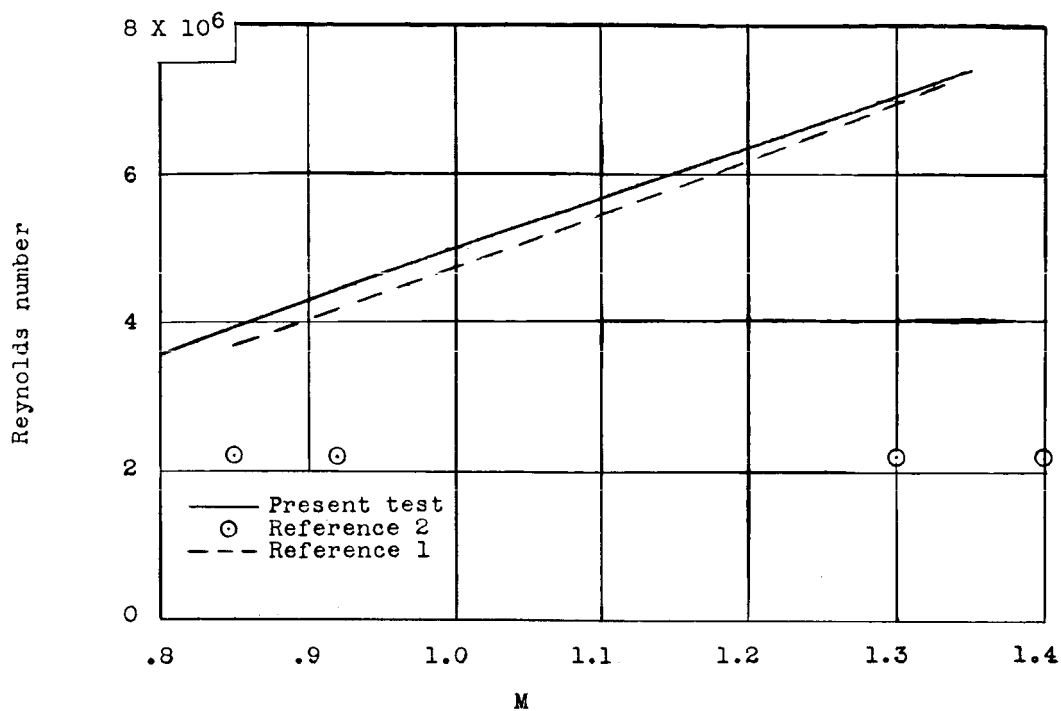
(a) Reynolds number.
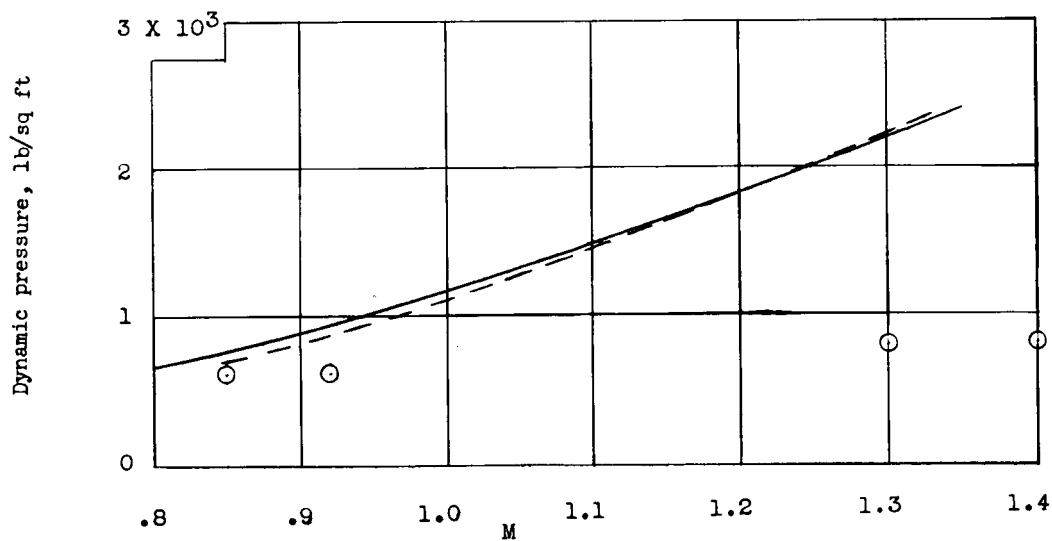
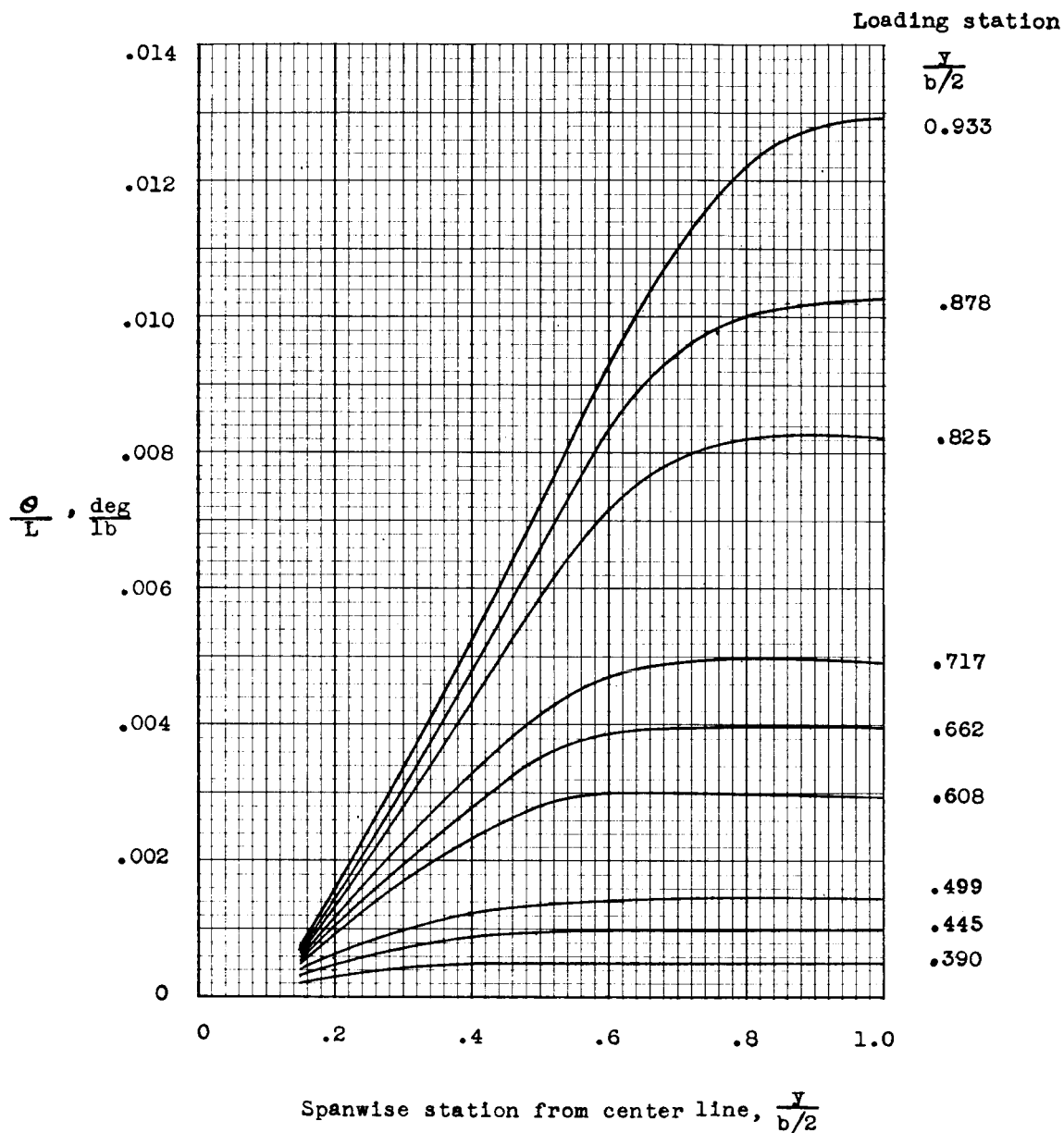(b) Dynamic pressure.

Figure 4.- Variation of Reynolds number and dynamic pressure.

Figure 5.- Streamwise influence coefficients for the duralumin wing due to loads applied along the 30-percent-streamwise-chord line and at the spanwise stations indicated.
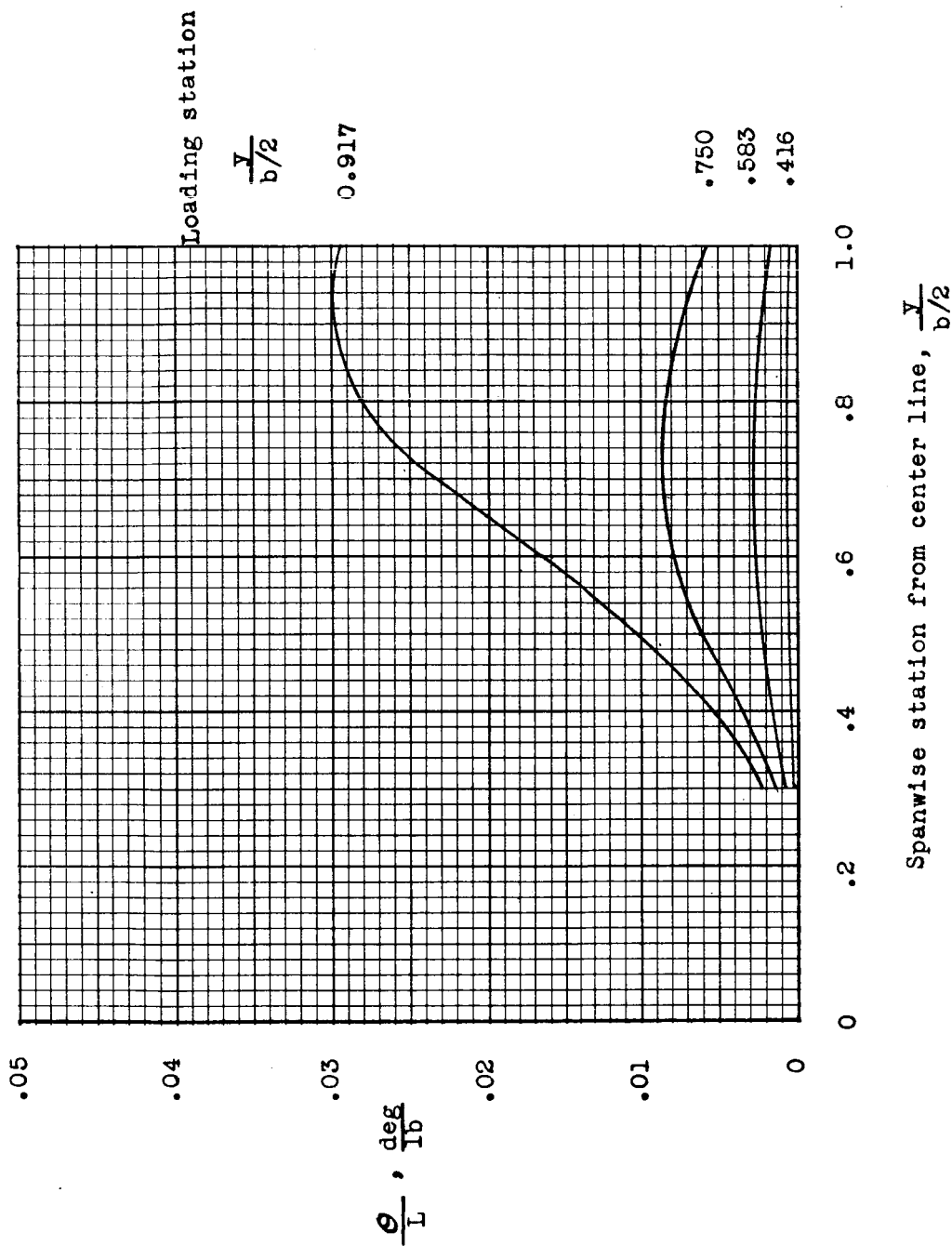
Figure 6.- Streamwise influence coefficients for the magnesium vertical
tail due to loads applied along the 40-percent-streamwise-chord line.
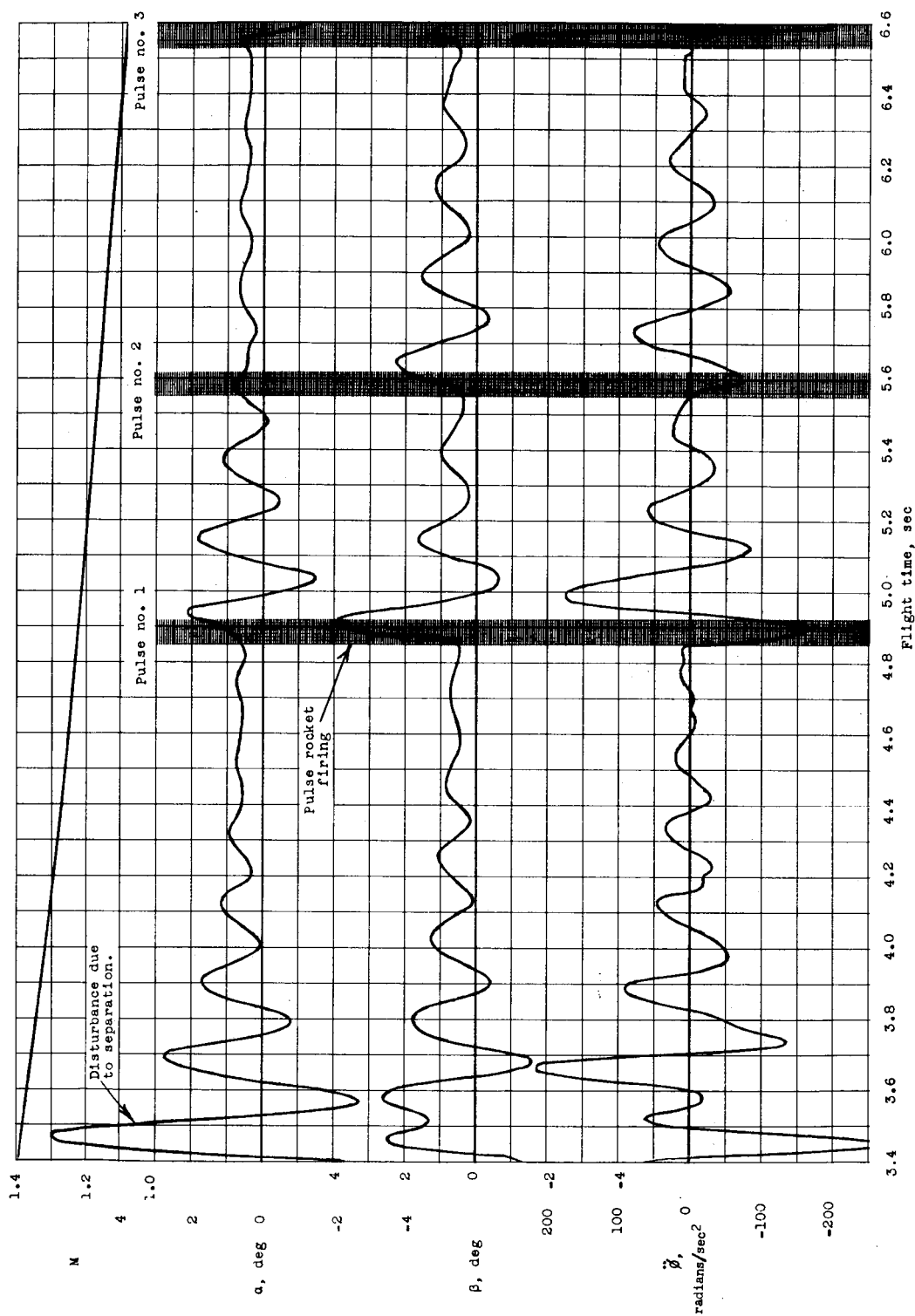
Figure 7.- Time histories of Mach number, angle of attack, angle of side-
slip, and rolling acceleration.
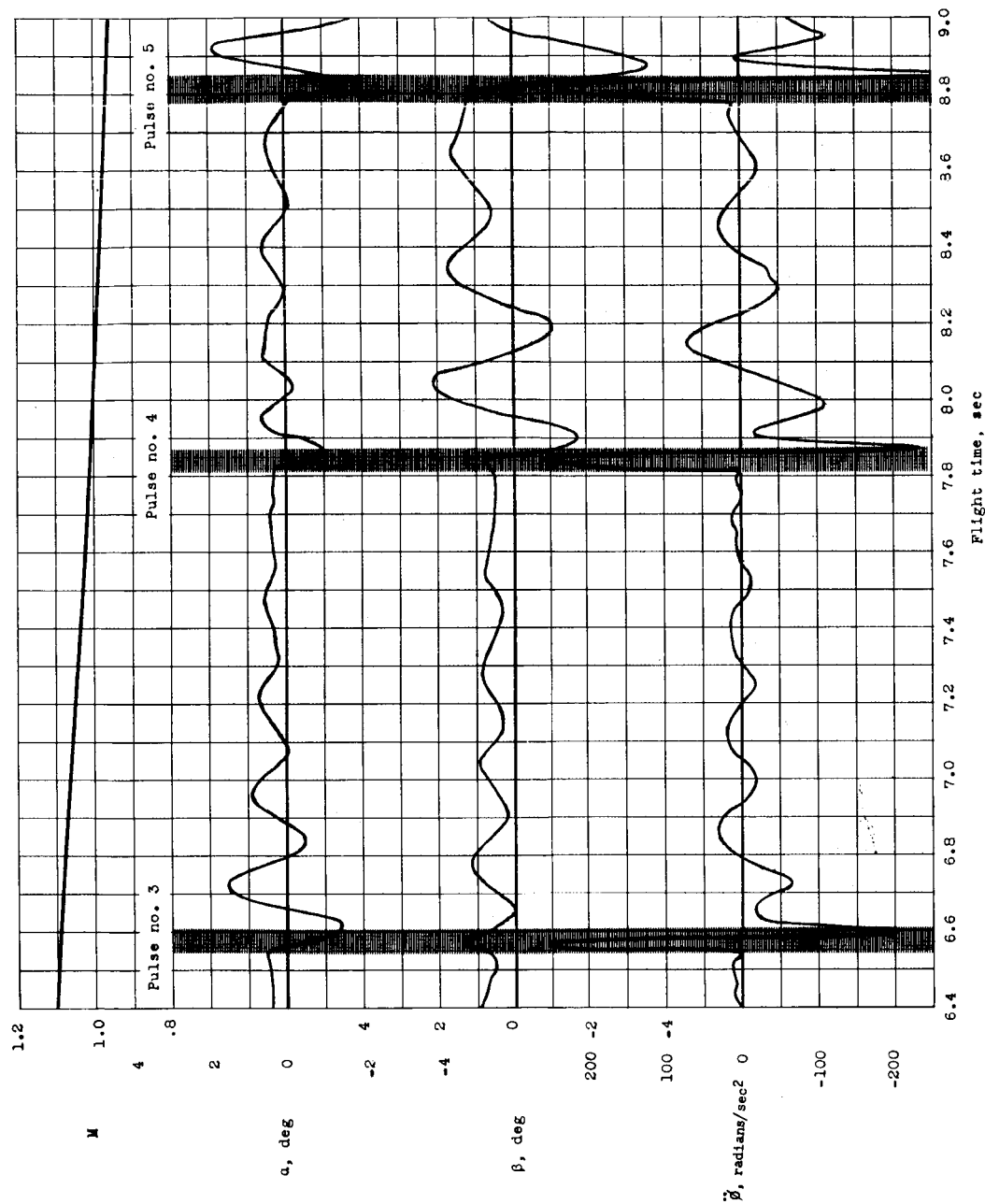
Figure 7.- Continued.

Figure 7.- Concluded.

$-\left|\dfrac{C_Y}{\beta}\right|$ $-\dfrac{mV}{qS}\,a\left|\dfrac{\ddot{\emptyset}}{\beta}\right|$

Assume weight vector = 0.

Solve for $\left|\dfrac{\dot{\psi}}{\beta}\right|$ and direction of $\dot{\psi}$

and for $\left|\dfrac{\ddot{\psi}}{\beta}\right|$ and direction of $\ddot{\psi}$.

$\dfrac{mV}{qS}\left|\dfrac{\dot{\psi}}{\beta}\right|$

$\dfrac{mV}{qS}\left|\dfrac{\dot{\beta}}{\beta}\right|$

$\tan^{-1}\dfrac{\omega}{a}$

→ Direction of β

Side-force equation: $\dfrac{mV}{qS}\left|\dfrac{\dot{\beta}}{\beta}\right| + \dfrac{mV}{qS}\left|\dfrac{\dot{\psi}}{\beta}\right| - \dfrac{mV}{qS}\,a\left|\dfrac{\ddot{\emptyset}}{\beta}\right| - \dfrac{C_Y}{\beta} = 0$

$-C_{l_r}\dfrac{b}{2V}\left|\dfrac{\dot{\psi}}{\beta}\right|$ C_{l_β}

$\dfrac{I_x}{qSb}\left|\dfrac{\ddot{\emptyset}}{\beta}\right|$

$-C_{l_p}\dfrac{b}{2V}\left|\dfrac{\dot{\emptyset}}{\beta}\right|$

Use estimated value of C_{l_p}.

Solve for C_{l_r} and C_{l_β}.

For present test I_{xz} term equals 0

Also $C_{Y_p} = C_{Y_r} = 0$

Rolling-moment equation $\dfrac{I_x}{qSb}\left|\dfrac{\ddot{\emptyset}}{\beta}\right| - \dfrac{I_{xz}}{qSb}\left|\dfrac{\ddot{\psi}}{\beta}\right| - C_{l_r}\dfrac{b}{2V}\left|\dfrac{\dot{\psi}}{\beta}\right| - C_{l_p}\dfrac{b}{2V}\left|\dfrac{\dot{\emptyset}}{\beta}\right| - C_{l_\beta} = 0$

$\dfrac{I_z}{qSb}\left|\dfrac{\ddot{\psi}}{\beta}\right|$ $-\left(C_{n_r} - C_{n_{\dot{\beta}}}\right)\dfrac{b}{2V}\left|\dfrac{\dot{\psi}}{\beta}\right|$ $C_{n_p} = -0.1$ $-C_{n_p}\dfrac{b}{2V}\left|\dfrac{\dot{\emptyset}}{\beta}\right|$

$C_{n_p} = +0.1$

Assume values for C_{n_p}.

Solve for $\left(C_{n_r} - C_{n_{\dot{\beta}}}\right)$ and C_{n_β}.

$-C_{n_\beta}$

Yawing-moment equation $\dfrac{I_z}{qSb}\left|\dfrac{\ddot{\psi}}{\beta}\right| - \dfrac{I_{xz}}{qSb}\left|\dfrac{\ddot{\emptyset}}{\beta}\right| - C_{n_p}\dfrac{b}{2V}\left|\dfrac{\dot{\emptyset}}{\beta}\right| - \left(C_{n_r} - C_{n_{\dot{\beta}}}\right)\dfrac{b}{2V}\left|\dfrac{\dot{\psi}}{\beta}\right| - C_{n_\beta} = 0$

Figure 8.- Typical vector plots of the equations of motion.
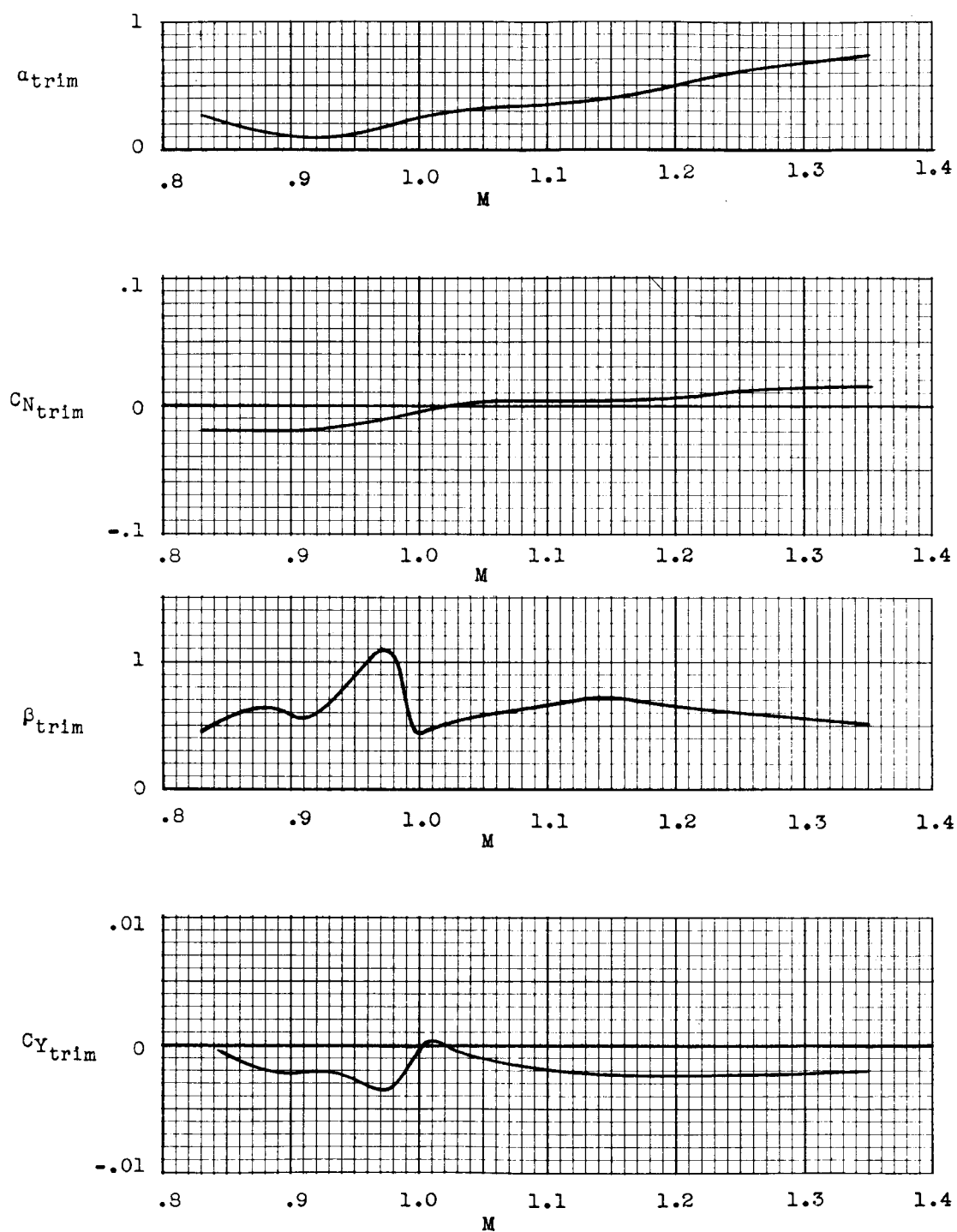
Figure 9.- Longitudinal and lateral trim characteristics.
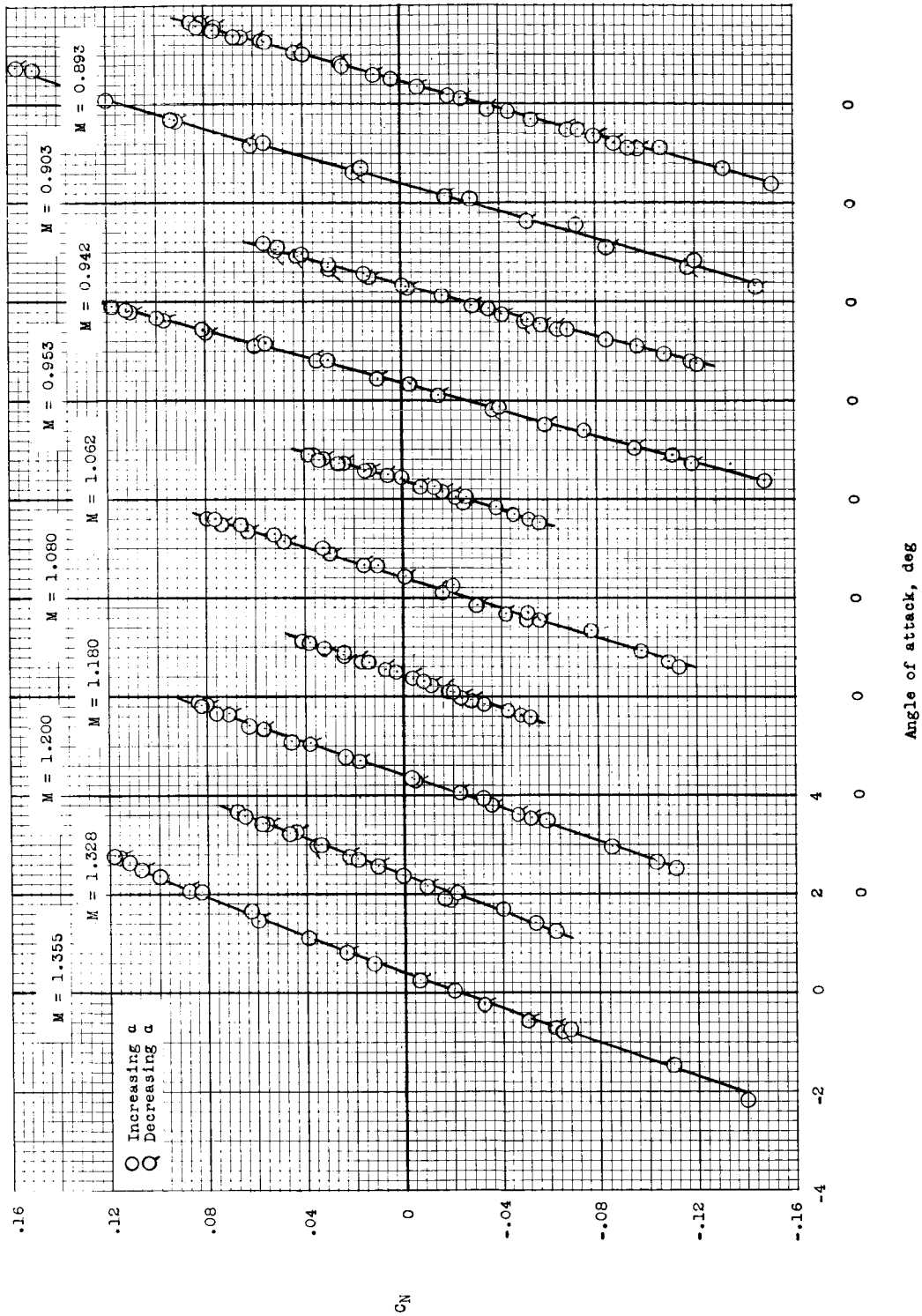
Figure 10.- Variation of normal-force coefficient with angle of attack
for various Mach numbers.
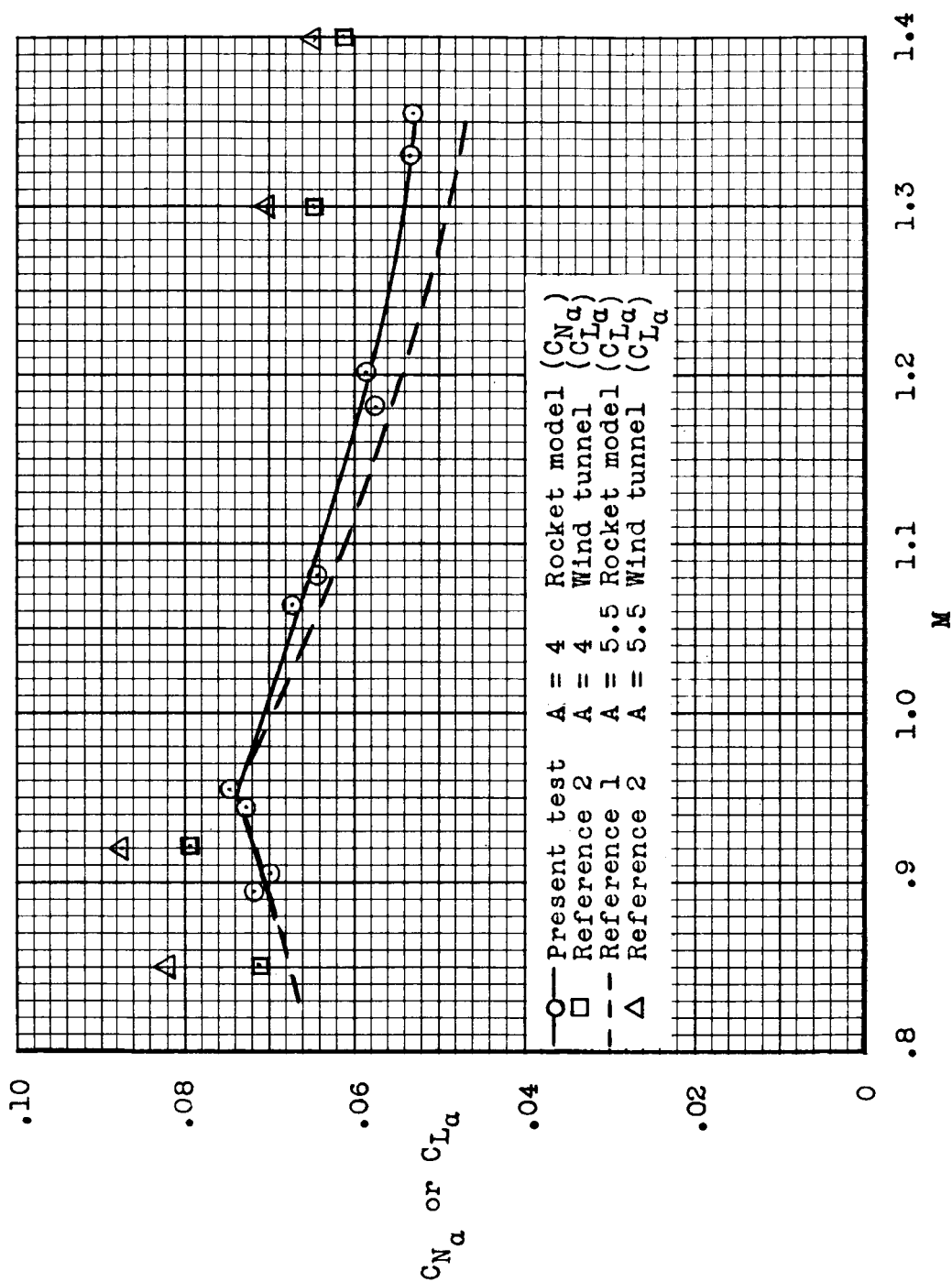
Figure 11.- Variation of normal-force-curve and lift-curve slope with Mach number.
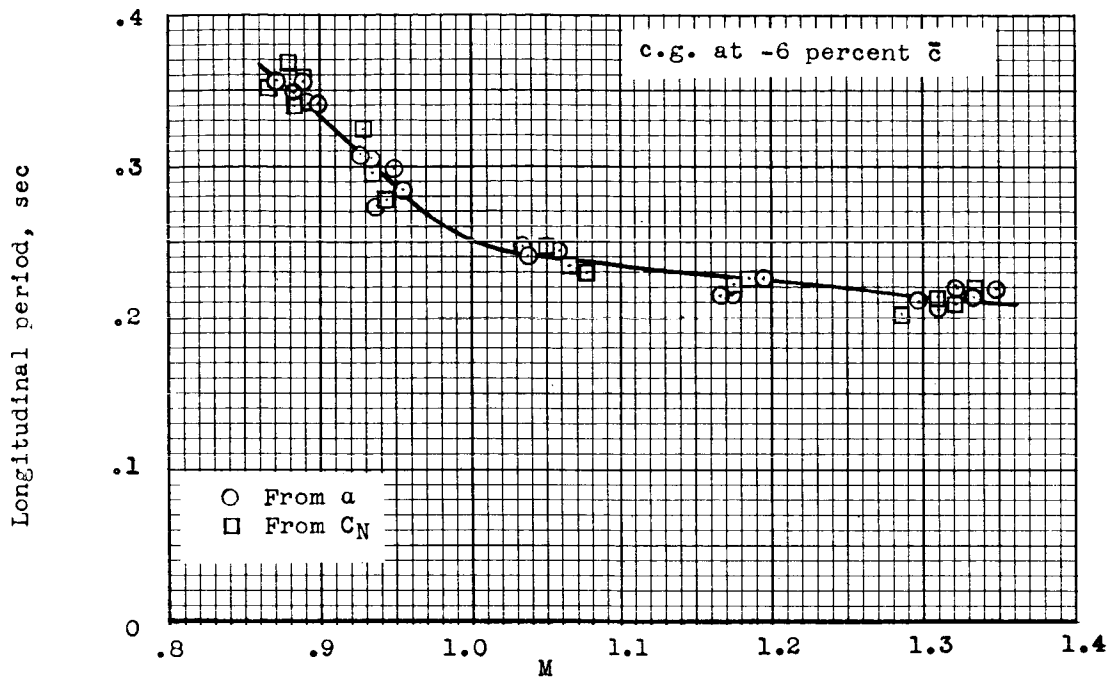
(a) Longitudinal period.
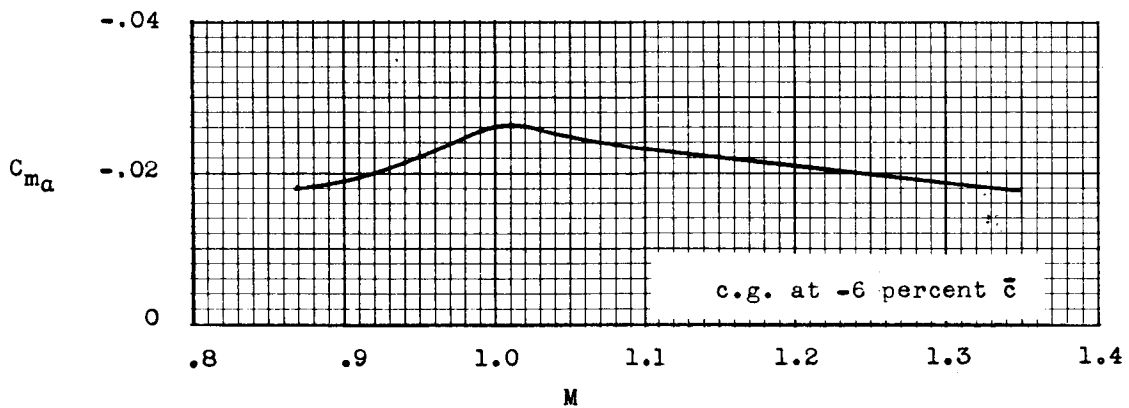
(b) Static stability derivative.

Figure 12.- Variation of longitudinal period and static stability deriva-
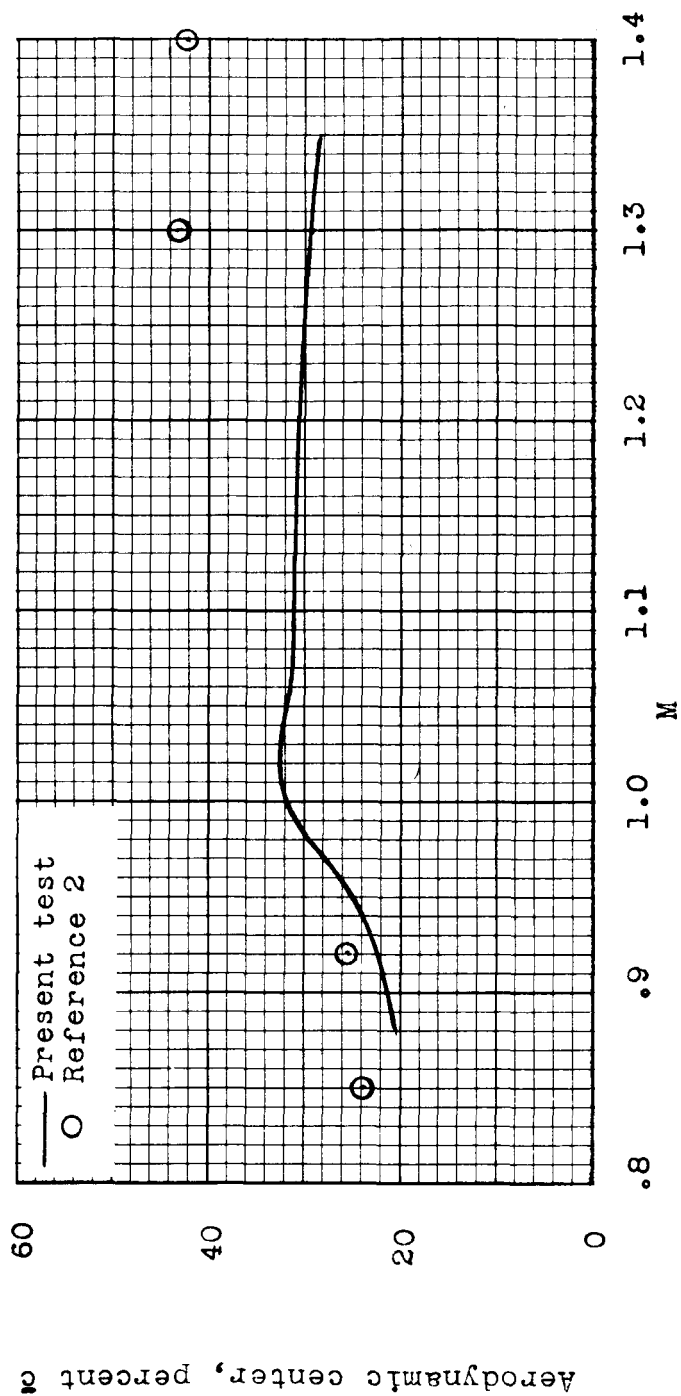tive with Mach number.

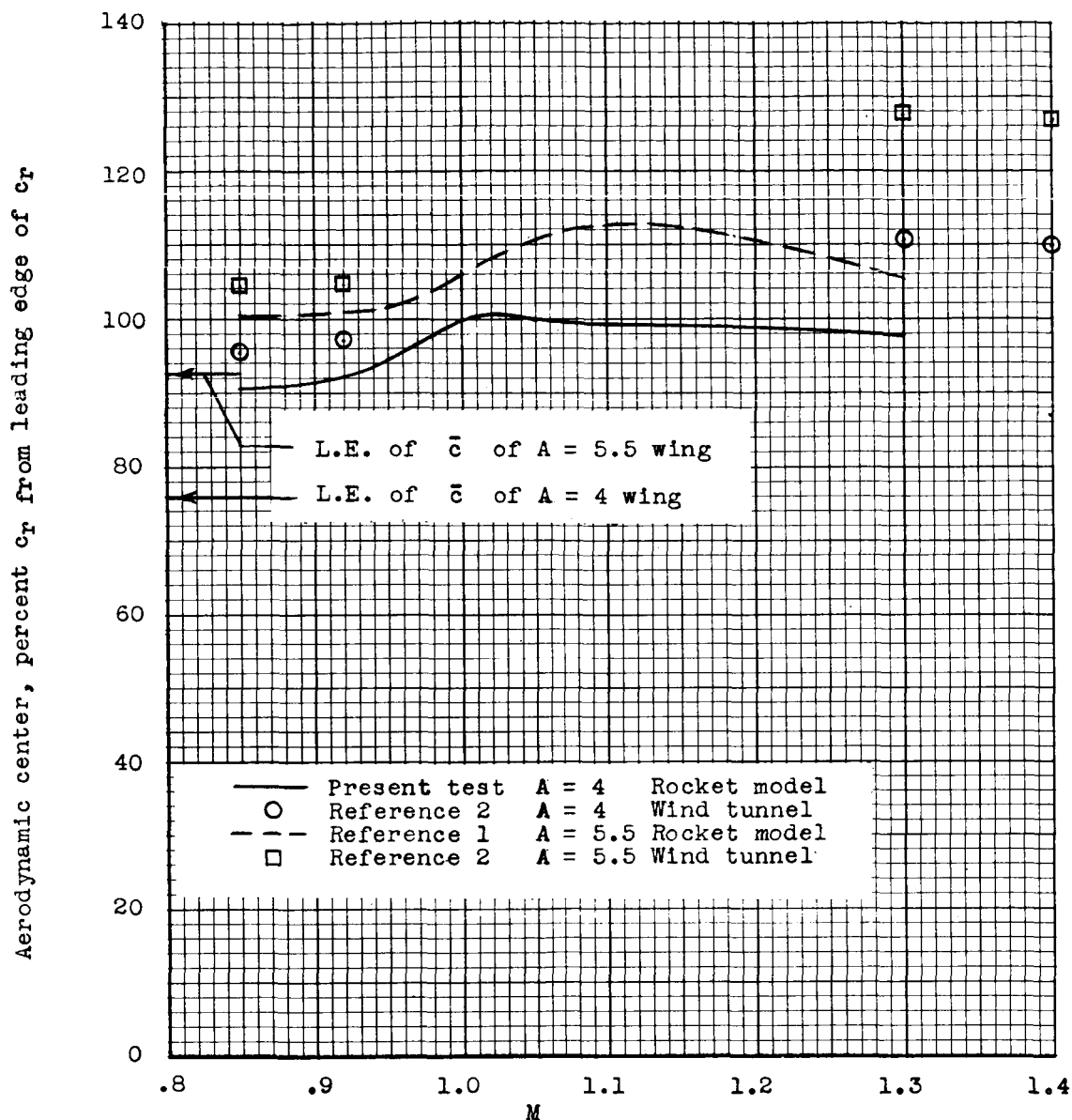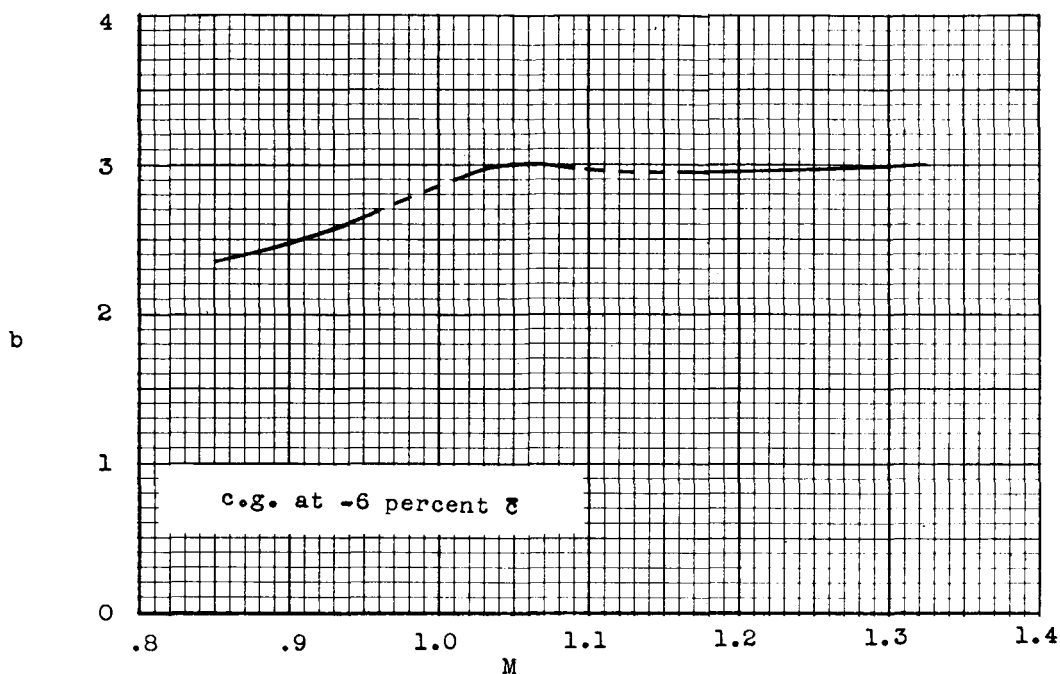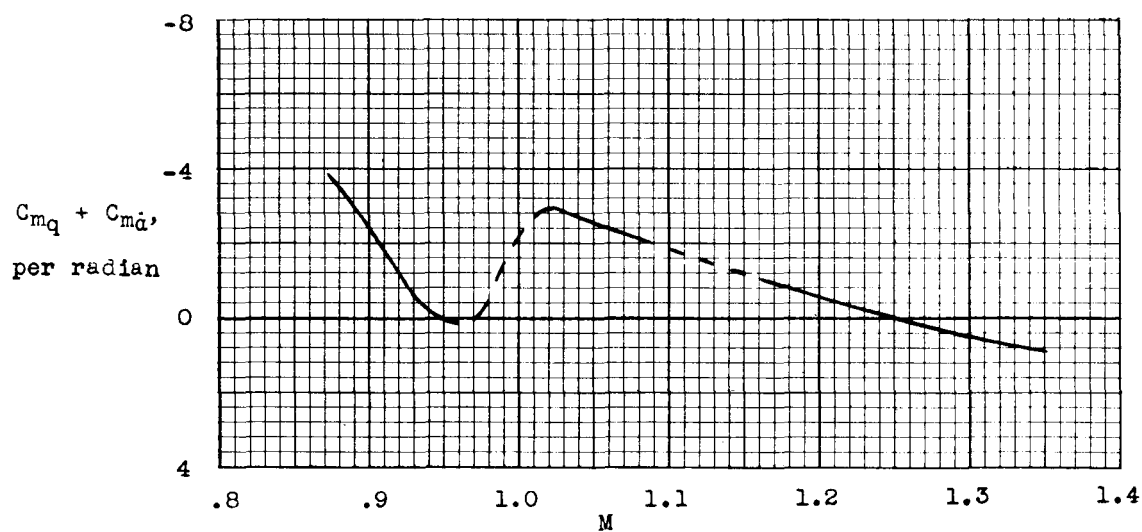Figure 13.- Variation of aerodynamic-center location with Mach number.

Figure 14.- Comparison of aerodynamic centers for the present test model
and referenced models. Aerodynamic-center locations are in percent
of root chord back of leading edge of root chord.

(a) Total damping factor.

(b) Pitch damping coefficients.

Figure 15.- Longitudinal damping characteristics.
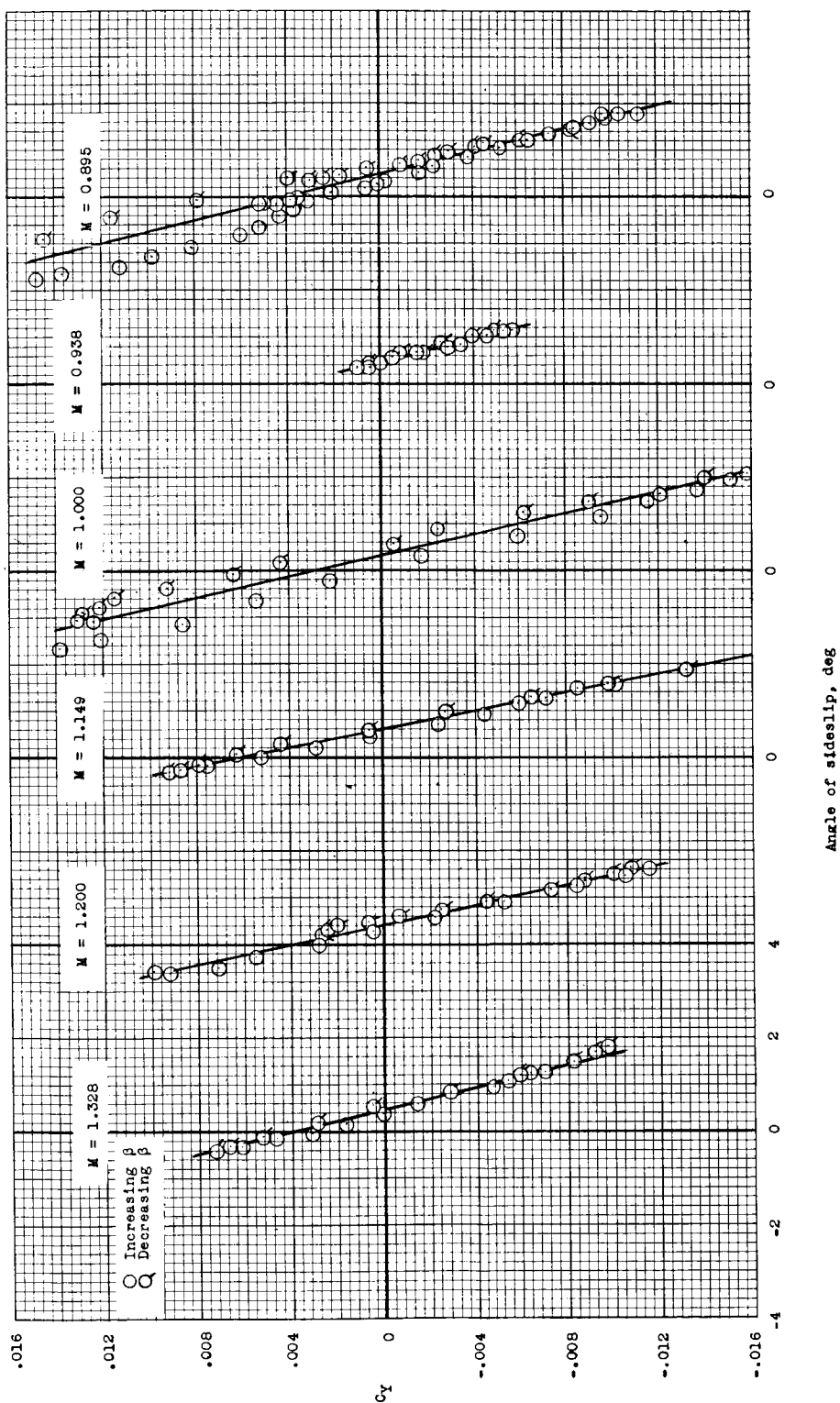
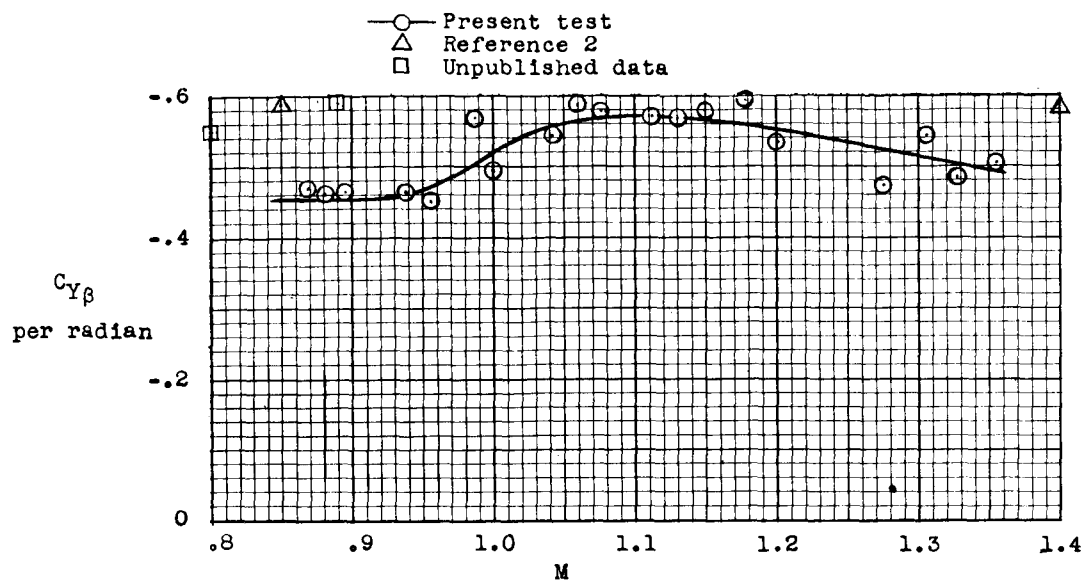Figure 16.- Typical variation of side-force coefficient with angle of sideslip.
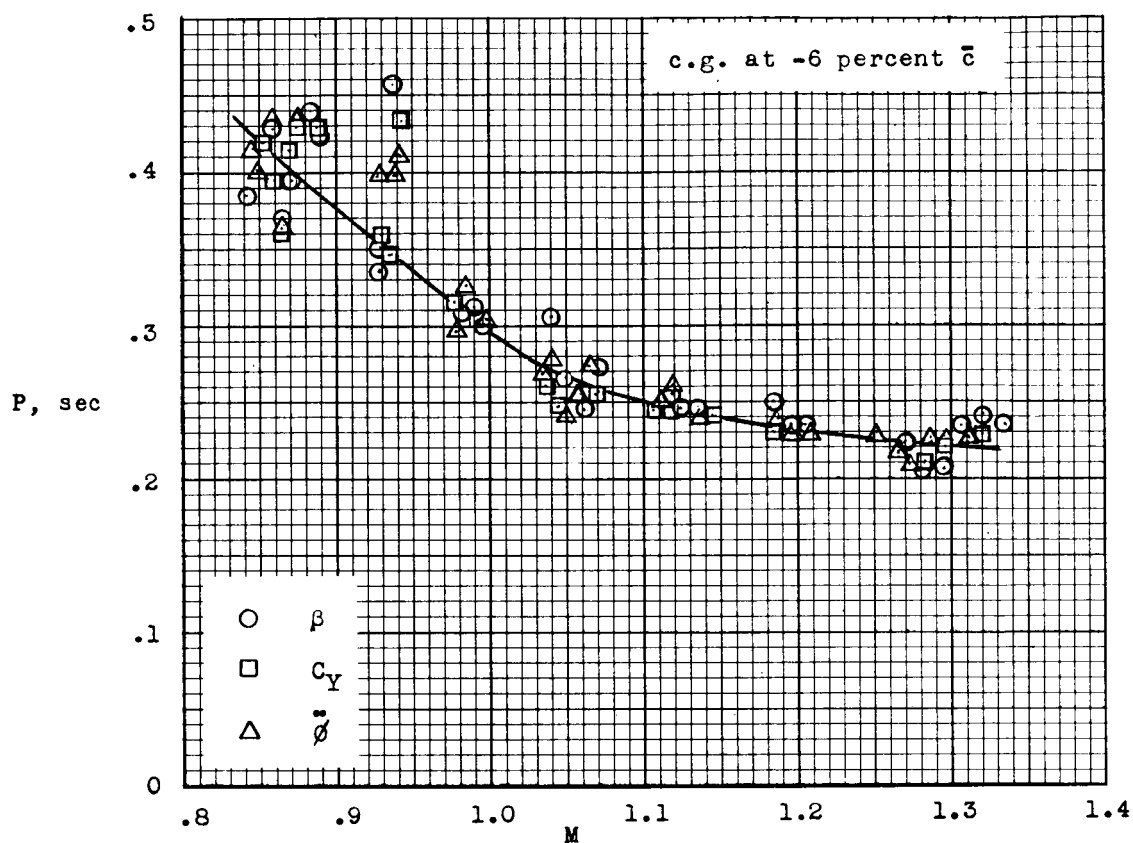
(a) Lateral periods.
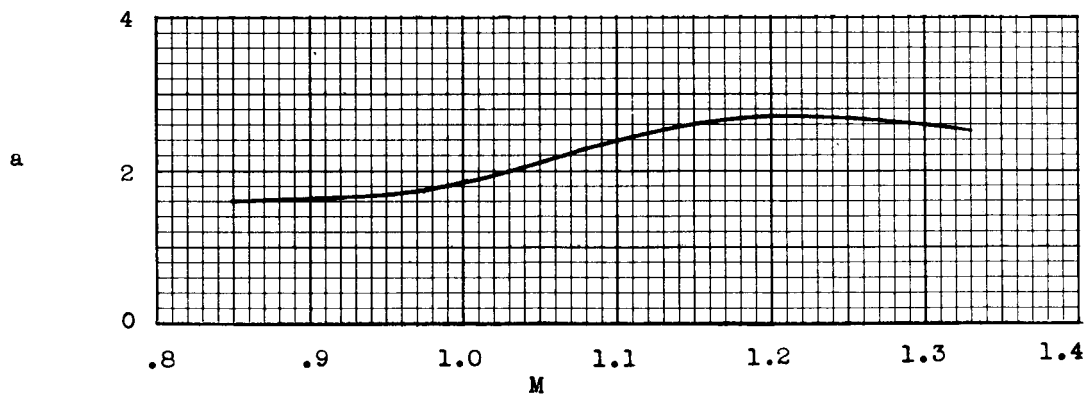
(b) Lateral damping factor.
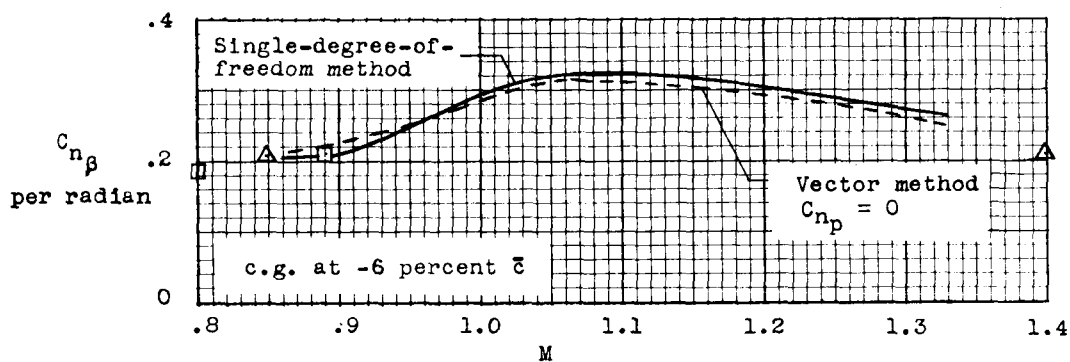
Figure 17.- Lateral period and total damping factor.
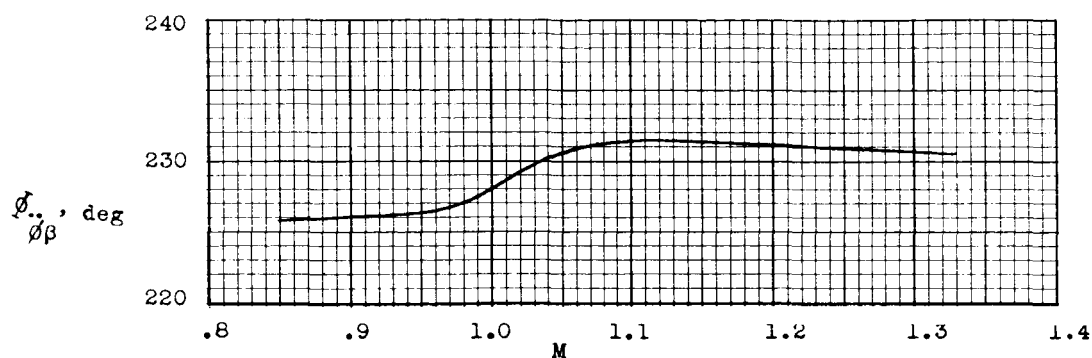
(a) Phase angle between $\overset{..}{\phi}$ and β.
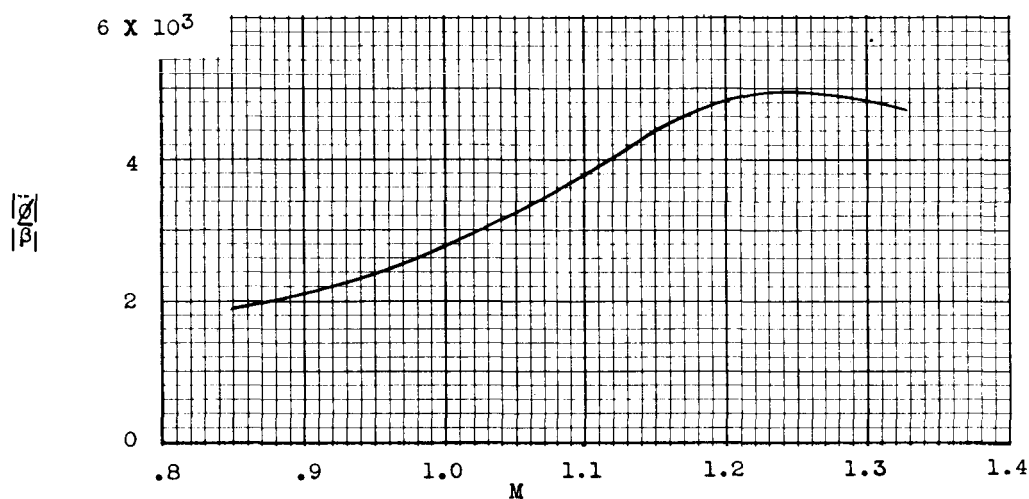
(b) Amplitude ratio of $\overset{..}{\phi}$ to β.
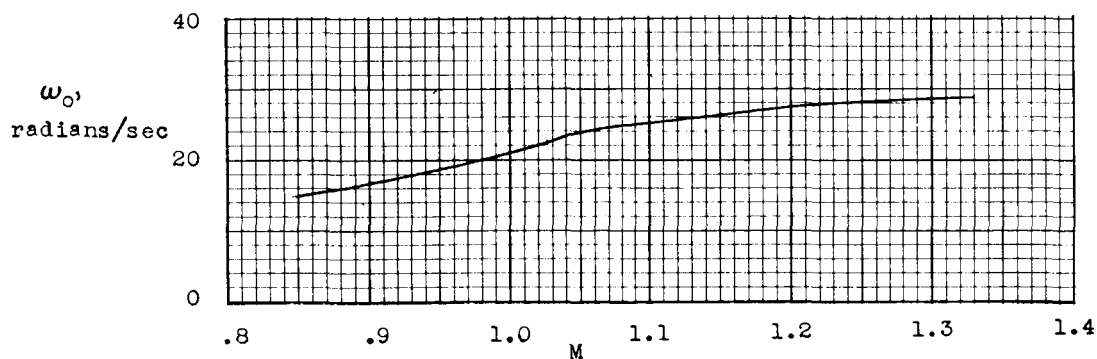
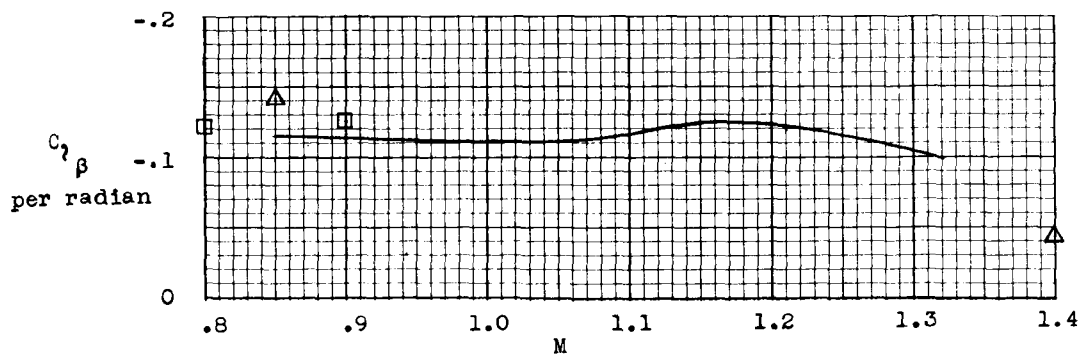(c) Undamped natural circular frequency.

Figure 18.- Relationships between $\overset{..}{\phi}$ and β and undamped natural circular frequency.
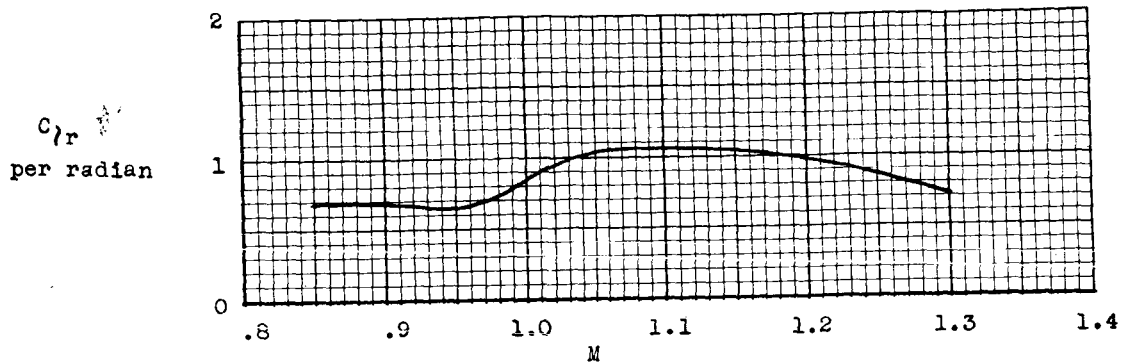
(a) Side-force derivative.
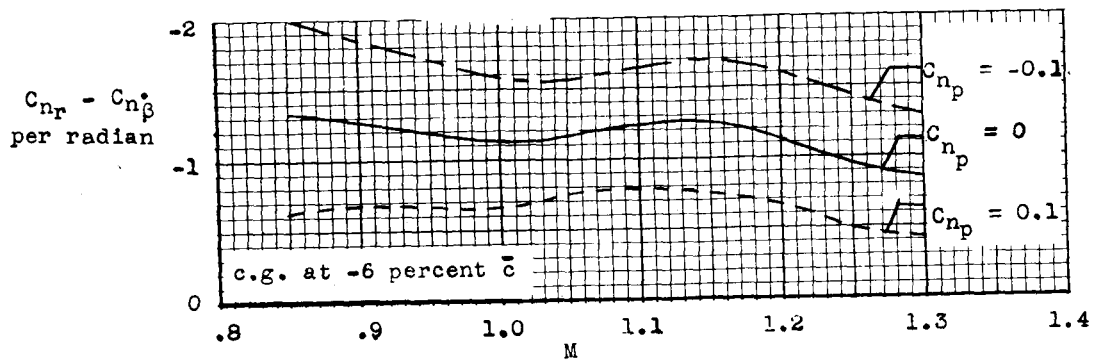
(b) Directional stability derivative.

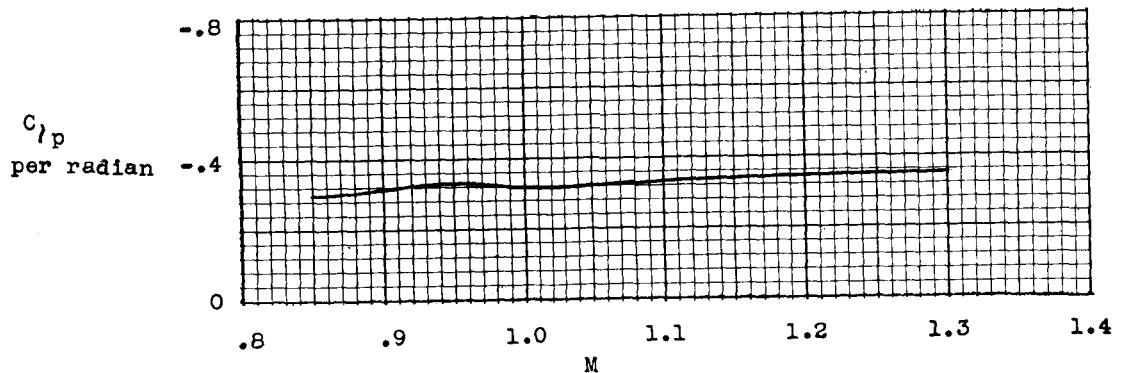(c) Effective dihedral derivative.

Figure 19.- Variation of sideslip derivatives with Mach number.

c_{l_r} per radian

2

1

0

.8   .9   1.0   1.1   1.2   1.3   1.4

M

(a) Rolling-moment-due-to-yawing derivative.

$c_{n_r} - c_{n_{\dot\beta}}$ per radian

-2

-1

0

$c_{n_p} = -0.1$

$c_{n_p} = 0$

$c_{n_p} = 0.1$

c.g. at -6 percent $\bar{c}$

.8   .9   1.0   1.1   1.2   1.3   1.4

M

(b) Damping-in-yaw derivative.

c_{l_p} per radian

-.8

-.4

0

.8   .9   1.0   1.1   1.2   1.3   1.4

M

(c) Estimated damping-in-roll derivative.

Figure 20.- Variation of moment derivatives due to yawing and of the
estimated damping-in-roll derivative.